PROCEEDINGS, Thirty-Seventh Workshop on Geothermal Reservoir Engineering
Stanford University, Stanford, California, January 30 - February 1, 2012
SGP-TR-194

THE EFFECTS OF TEMPERATURE DEPENDENT CONDUCTIVITY ON BASIN SCALE HEAT FLOW

S. Quenette[1], L. Moresi[1], C. O'Neill[2], C. Danis[2]

1. School of Mathematical Sciences
Monash University
Melbourne, Victoria, 3800, Australia
e-mail: steve.quenette@gmail.com
2. *GEMOC ARC National Key Centre, Department of Earth and Planetary Sciences*
Macquarie University
Sydney, New South Wales, 2109, Australia

ABSTRACT

We present a methodology for calibrating numerical models of deep crustal heat flow, which incorporate structural information at the thousand-kilometer scale whilst maintaining a quantification of uncertainty. Geological structural interpretations are increasingly the product of geological and geophysical inversion methods, and include some quantification of the propagation of uncertainty through the modeling process to the output. A problem arises in the scale of computation needed to meet these requirements, which can quickly saturate computational resources readily available.

In this paper we show an intuitive example of the use of forward models to analyse the effect of variation in a single aspect of a model parameterization: the non-linearity resulting from temperature dependence of thermal diffusivity. Our starting point is the Sydney-Gunnedah basin. In the context of basin geometry, how sensitive is the model response to variations in temperature dependent conductivity?

INTRODUCTION

We now have the capability to model heat flow in high-resolution models of basins and systems of basins. There is an increasing interest in using these models to *assess* resource potential at a regional scale and to provide guidance for exploration drilling programs so as to maximize information about the subsurface temperature distribution.

The study of geothermal potential at the reservoir scale is a mature field. For example the method of 1d heat flow with assimilation of surface heat flow measurements (e.g. Chopra & Holgate 2005 within an Australian context). Other methods account for complexities such as 2d & 3d geological structure, subsurface fluid-flow and phase reactions (e.g. Wellmann 2010), material anisotropy and anisotropy resulting from fine-scale layering, and non-linearity.

Geological structural interpretations are increasingly the product of geological and geophysical inversion methods, and include some quantification of the propagation of uncertainty through the modeling process to the output. Heat flow modeling requires calibration and hence can be considered a nested inversion for petrophysical properties.

A problem arises in the scale of computation needed to meet these requirements. Australian basins of interest to geothermal explorers are of the order of 100s to 1000s of square kilometers with some stratigraphic units such as coal seams of the order of less than 10s of meters thick. Capturing the uncertainty in the structure and composition of the subsurface requires us to produce ensembles of regional basin models at a resolution which captures the 1-10s meter vertical scale (including mesh refinement), within an inversion context. In computational terms, this equates to resolutions of 10^6-10^9 elements over 100-1000s of concurrent processes, and over 1000-10000s of realizations.

These are very large computational problems, and quickly saturate computational resources readily available.

The goal then is to ensure both (a) each realization completes in a few seconds and (b) a reduction in the number of required realizations (whilst maintaining confidence in the result). If we set an expectation of 1000 realizations for the purposes of calibration, this places emphasis on the ability to explore for measures that capture model response to variants. Better measures will capture more constraint information, which in turn encourages measures that relate to available near surface observables.

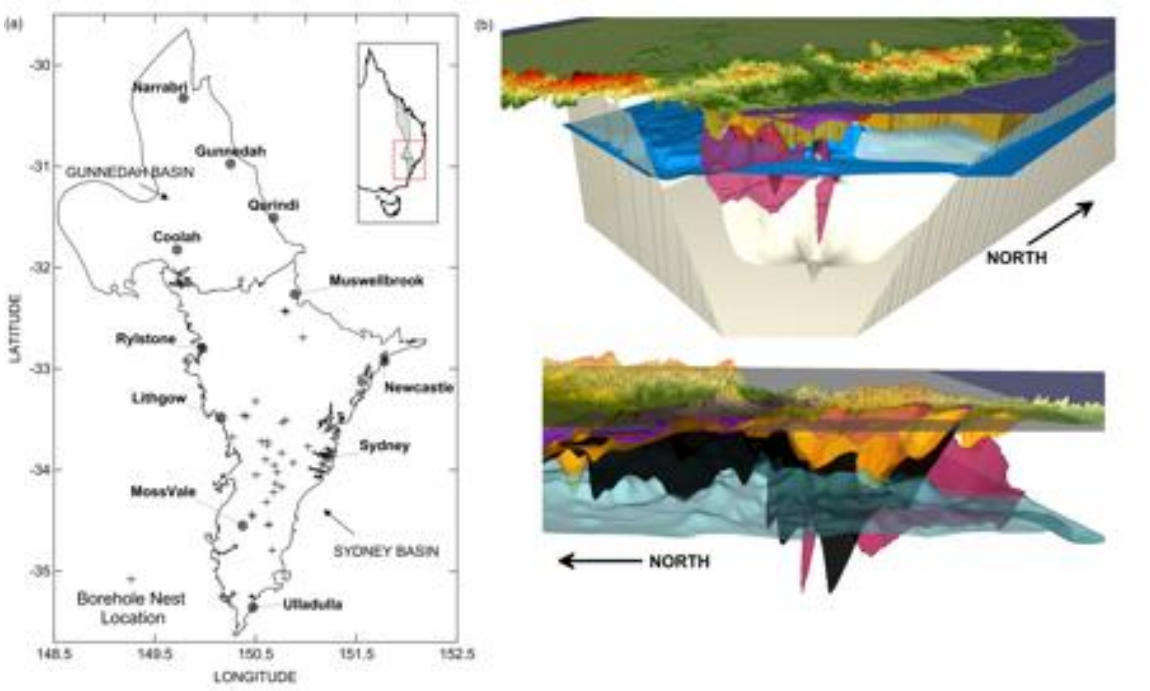

Figure 1 - Sydney-Gunnedah Basin model area showing (a) location of equilibrated drill holes, and (b) 3D geological model views from *Underworld,* with surface elevation, coal layers, volcanics and basement. The vertical direction is exaggerated 10times.

It is worth noting the role played by 3d structural models in this scenario. Structure and composition are the dominant controls on the subsurface temperature distribution. Structural information also is significantly denser than geothermal (borehole) observables. This provides an opportunity to treat structural realizations as truth-values into a geothermal inversion, and thus including potential field geophysics into the inversion.

In this paper we show an intuitive example of the use of forward models to analyse the effect of variation in a single aspect of a model parameterization: the non-linearity resulting from temperature dependence of thermal diffusivity.

High temperatures at depth may result from blanketing by low conductivity sedimentary layers or coal measures. Furthermore, we intuitively expect that blanketing will be enhanced if thermal diffusivity is reduced at high temperatures. This effect is known to be important at the scale of the mantle and lithosphere (e.g. Hauck et al, 1999, Dubuffet et al, 1999, van den Berg 2001). However, in the context of basin geometry, how sensitive is the model response to variations in temperature dependent conductivity? In particular, is the response non-linear or of a nature such that the calibration or inversion methodology needs to be reconsidered?

In the following experiments we assume a single geological architecture, but in the context that the methods developed and used here would naturally integrate into a unified geological, geophysical and geothermal inversion. Our starting point is the Danis el al (2010,2011a) model of the Sydney-Gunnedah basin.

HEAT FLOW BASE-LINE MODEL

In a recent study (Danis et al 2012, in prep), we made a preliminary investigation into methods for quantifying uncertainty in the calibration of continental scale thermal models. A brief of this method, tailored to following experiment is described here.

We applied the tool *Underworld-GT* (Quenette & Moresi 2010), a toolbox of *Underworld* (Moresi et al 2007), to solve the non-linear heat flow equation. *Underworld-GT* has the ability to scale to 1000s of processes, load 3d models from goCAD, GeoModeller and CSV surface exports, and pre- and post- process various borehole data for calibration. In this work we improve the latter.

The Sydney-Gunnedah basin thermal model covers a volume area of over 600 km by 300 km to a depth of 12 km. We employ a mesh refinement that guarantees a maximum element size of 1130m in the lateral directions, and 11m in the vertical direction. The refined region extends 700 to -2000 mAHD vertically, covering the calibration drill core data both laterally and vertically. This choice ensures that

the mesh refinement average error is less than 0.01°C. The resultant resolution is 240x318x438 elements. Using 3gb of memory per core, Underworld-GT requires 128cores to solve a heat flow model realisation in 4±1 minutes.

The temperature dependent conductivity data in the baseline model are an application of the Clauser and Huenges (1995) compilation — a large database of thermal conductivity measurements on various rocks under different temperature conditions. Their values are used to construct piecewise-linear conductivity-temperature curves material (m) is given by:

$$K_m(T) = \begin{cases} K_0 - \dfrac{(T - T_0)(K_0 - K_{crit})}{T_{crit} - T_0}, & T_0 < T < T_{crit} \\ K_{crit}, & T \geq T_{crit} \end{cases} \quad (1)$$

Where T is the temperature and K the thermal conductivity. K_0 and K_{crit} are the thermal conductivity at surface temperature and at T_{crit}, respectively. T_{crit} is the temperature above which the thermal conductivity is held constant, T_0 is the surface temperature.

The calibration is posed as an inverse problem where parameter and ensemble distributions describe model certainty. A set of realizations was incrementally generated from random samples of each parameter based on a reasonable initial range or mean. Over the course of the inversion, (quasi-random) parametric, random over the range and normal distributions were used in a strategy to reduce the total number of realizations required given the computational footprint of the simulation. The direction of search through the constraint iterations was guided by an initial uni-variant parameter analysis. For example, for the 'Greta' unit, reasonable values of K_0 have relatively little influence, and hence the parameter is effectively removed as a variant. Many heat production parameters are similar.

The calibration is achieved through a constraint model to fit against 44 equilibrated boreholes (approximately 260 temperature points), weighted between mean, variance and three levels of equilibrium confidence. Borehole samples within near surface aquifers were omitted. Realizations with a result beyond a threshold are discarded from the developing ensemble. The boundary conditions of basal and surface boundary conditions are also considered. From a resultant ensemble of realizations that satisfy the threshold of 0.1 on the constraint model, model *155* is assumed as the baseline for further experiments (see Table 1 in appendix).

THE EXPERIMENT

In this experiment, we assume T_0 for all materials to be the surface temperature, and T_{Crit} for all materials to be close to the bottom of the domain (approximately 300°C). This forces the model temperatures into the linear gradient of the conductivity model, and therefore we only vary K_{Crit}. From the uni-variant study, only K_{Crit} from the Lachlan Fault Belt causes significant variance on the resultant borehole temperatures.

Hence we study the significance of K_{Crit} of the basement below the Lachlan Fault Belt in further detail. Here we specifically vary it from 1.0 to 3.0 in 0.5 increments. We then take the linear regression between each of the successive five variations. The linear regression is performed on each of the 44 boreholes profiles. The boreholes are sampled every 10meters to create a profile of temperature, effective conductivity and subsequently three components of heat flow. See Figure 2 for the PPG8 borehole. Two further figures are provided in the appendix, showing other modes of conductivity change with depth. The borehole temperature and heat flow component regression is then analyzed, as the distribution in variance – see Figure 3 for temperature and the appendix for the components of heat flow.

To obtain these results we improved *Underworld-GT* to dump the effective conductivity and heat-flow components together with the geotherm profile.
We also created new geothermal model analysis software for rapid and automated analyses of ensemble results, which was lacking in Danis et al (2012).

PPG8

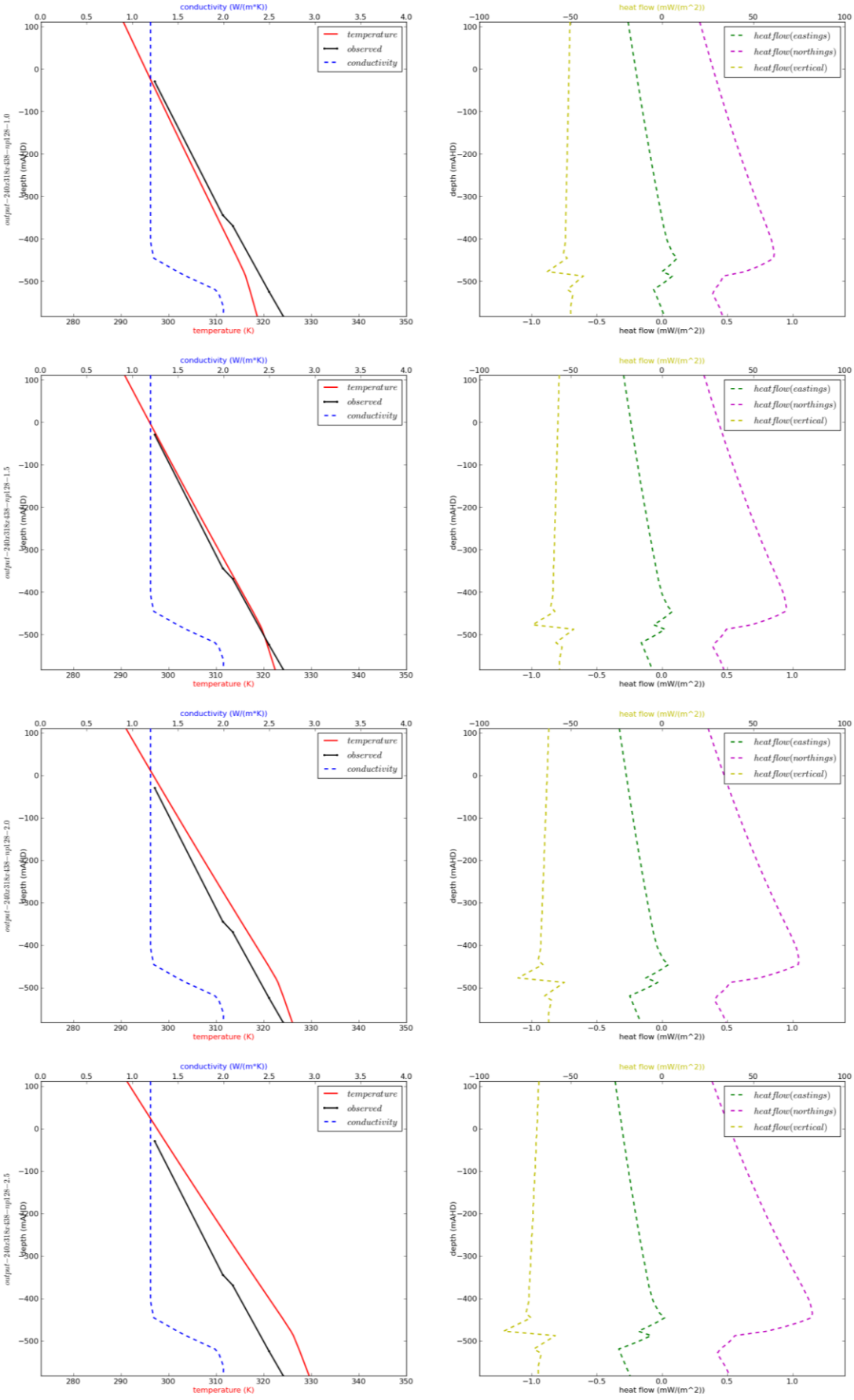
conductivity (W/(m*K))
temperature
observed
conductivity
temperature (K)
depth (mAHD)
heat flow (mW/(m^2))
heat flow(eastings)
heat flow(northings)
heat flow(vertical)
heat flow (mW/(m^2))
output~240x318x438~opt28~1.0
output~240x318x438~opt28~1.5
output~240x318x438~opt28~2.0
output~240x318x438~opt28~2.5

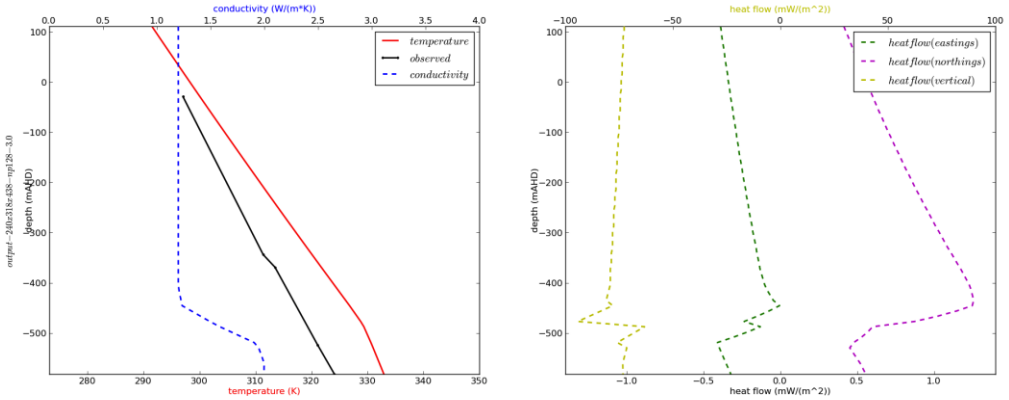

Figure 2 - Shows the temperature, conductivity, and heat flow component profile with depth for the borehole PPG8. The actual observed (source data) borehole geotherm is also shown in black. Each row is a model scenario in the experiment. The depth, thermal and heatflow scales are consistent in each graph. Note that the vertical heat flow scale is approximately x10 of the lateral flow. The analysis software can automatically generate such graphs for each borehole for each realization in one or many ensembles.

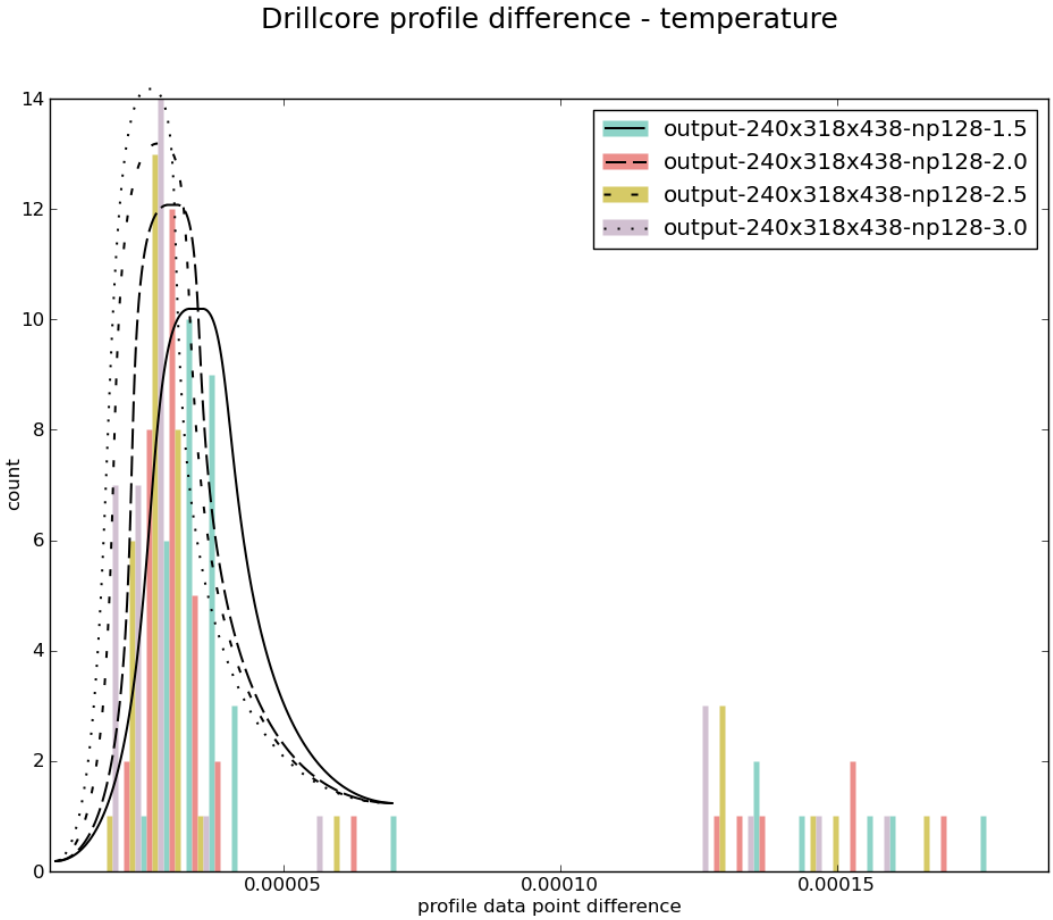

Figure 3 - Shows the standard error from a linear regression of borehole temperature for Lachlan Fault Belt K_{Crit} at 1.5 vs 1.0, 2.0 vs 1.5, 2.5 vs 2.0, and 3.0 vs 2.5. Annotated with black striped lines is an interpretation of fit for each of the four cases. As K_{Crit} is increases, the variance of borehole temperature tends to reduce.

DISCUSSION

The geotherm/heat-flow plots offer useful insight. As we see for the PPG8 borehole, the slope of the geotherm does vary considerably compared to the observed temperatures over the 700m. As K_{Crit} increases, the heat flow gradients increase. This behavior is generally exhibited across the 44 boreholes. There are also clear signs of refraction with boreholes with no material change (constant K_0) but have varying lateral heat flow. Regions of lateral heat flow are more affected by varying K_{Crit}.

Figure 3 shows a summary of the temperature variance in the experiment. It shows that as K_{Crit} is decreased, the variance between realizations trends towards increasing. There is an order of magnitude difference between the average variance of the K_{Crit}=1.5-2.0 and 2.5-3.0 models. The K_{Crit}=2.5-3.0 distribution is taller, narrower and at lower regression residuals compared to the successive decrements of K_{Crit}. Low values of K_{Crit} have a stronger control on the model.

A similar pattern is observed with the vertical component of heat flow, whereas the northings component weakly suggests the opposite where decreasing K_{Crit} decreases the variance. The eastings component has a similar variance across each of the comparisons. The vertical and eastings heat flow components are generally much larger than northings, and hence the net effect is consistent with the temperature comparison.

In the context of inversions, the trend suggests that for lower K_{Crit} values, the model-wide non-linearlity increases, and thus, the resolution of parameterization will increase.

However the results suggest that modeling temperature dependent conductivity within a complex 3d basin scale model is important. There is an observed increase in near–surface lateral heat flow.

CONCLUSION

We are able to model heat flow of large basin systems, and investigate aspects of parameter uncertainty. In particular, develop measures of the non-linearity of temperature dependence of thermal diffusivity that occur at depth, but measured near surface.

ACKNOWLEDGEMENTS

The computational work was performed using the NCI merit allocation p67 - “Energy driven understanding of deep geological resources”. We would also like to thank the Monash eResearch Centre for - the operations of our institutional computational facilities, hosting of the Underworld software development project, and Steve Quenette’s time on this project.

REFERENCES

van den Berg, A.P. Yuen, D. A., Steinbach, V. The Effects of Variable Thermal Conductivity on Mantle Heat-Transfer, Geophysical Research Letters, 28, 875-878, 2001

Chopra P. & Holgate F. 2005. A GIS analysis of temperature in the Australian crust. World Geothermal Congress, Turkey, 24-29 April 2005, Abstracts.

Clauser, C., Huenges, E., Thermal conductivity of rocks and minerals, in Rock Physics and Phase Relations, A handbook of physical constants. American Geophysical Union, pp. 105-126, 1995..

Dubuffet, F., Yuen, D.A. and M. Rabinowicz, Effects of a realistic mantle thermal conductivity on the patterns of 3-D convection, Earth Planet. Sci. Lett., 171, 401-409, 1999

Danis, C., O’Neill, C. and Lackie, M., Gunnedah Basin 3D architecture and upper crustal temperatures. Australian Journal of Earth Sciences, 57, 483-505, 2010.

Danis C., O’Neill C., Lackie M., Twigg L. and Danis A. 2011a. Deep 3D structure of the Sydney Basin using geophysical modelling. *Australian Journal of Earth Sciences* **58**, 517-542.

Danis C., Quenette S., O’Neill C., Mansour J., and Moresi L., An assessment of subsurface temperatures and uncertainty in 3D geothermal models of the Sydney-Gunnedah basin system, in prep 2012

Hauck, S.A. II, R.J. Phillips and A. M. Hofmeister: Variable conductivity: Effects on the thermal structure of subducting slabs, Geophysical Research Leters, vol. 26, no. 21, pp. 3257-3260, 1999

Hofmeister, A.M.: Mantle values of thermal conductivity and a geotherm from phonon lifetimes. Science 283, 1699-1706, 1999

Moresi L., Quenette S., Lemiale V., Meriaux C., Appelbe B., & Mulhaus H.-B. 2007. Computational approaches to studying non-linear dynamics of the crust and mantle. *Physics of the Earth and Planetary Interiors* **163**, 69-82.

Quenette S., Moresi L. Models based experimentation: numerical modelling of 3D basin scale architecture heat & fluid flow - AGU Fall Meeting Abstracts, 2010

Wellmann J.F., Horowitz F.G., Regenauer-Lieb K. 2010a. Influence of geological structures on fluid and heat flow fields. Proceedings - Thirty-Fifth Workshop on Geothermal Reservoir Engineering Stanford University, Stanford, California, February 1-3, 2010.

APPENDIX

Table 1 - The parameter values from realization "155" provided as indicative petrophysical and boundary conditions results from the inversion. These are used as a baseline model for the experiment.

Parameter	value
K_0 (W/m-K)	
Sediment	2
PCM	1.2
Basement below the Lachlan Fault Belt	3
Basement below Hunter Mooki	3
Maules	0.3
Greta	0.3
Onshore volcanic	3
Offshore volcanic	3
K_{Crit} (W/m-K)	
Sediment	1.5
PCM	0.2
Basement below the Lachlan Fault Belt	1.5
Basement below Hunter Mooki	2.25
Maules	0.2
Greta	0.2
Onshore volcanic	2.25
Offshore volcanic	2.25
T_{Crit} (K)	
All materials	573.15
Heat production ($\mu W/m^3$)	
Sediment	1.25
PCM	1.25
Basement below the Lachlan Fault Belt	2.00
Basement below Hunter Mooki	2.00
Maules	1.25
Greta	1.25
Onshore volcanic	0.5
Offshore volcanic	0.5
Thermal boundary conditions (K)	
Surface	288.15
Basal	618.15

GBD1

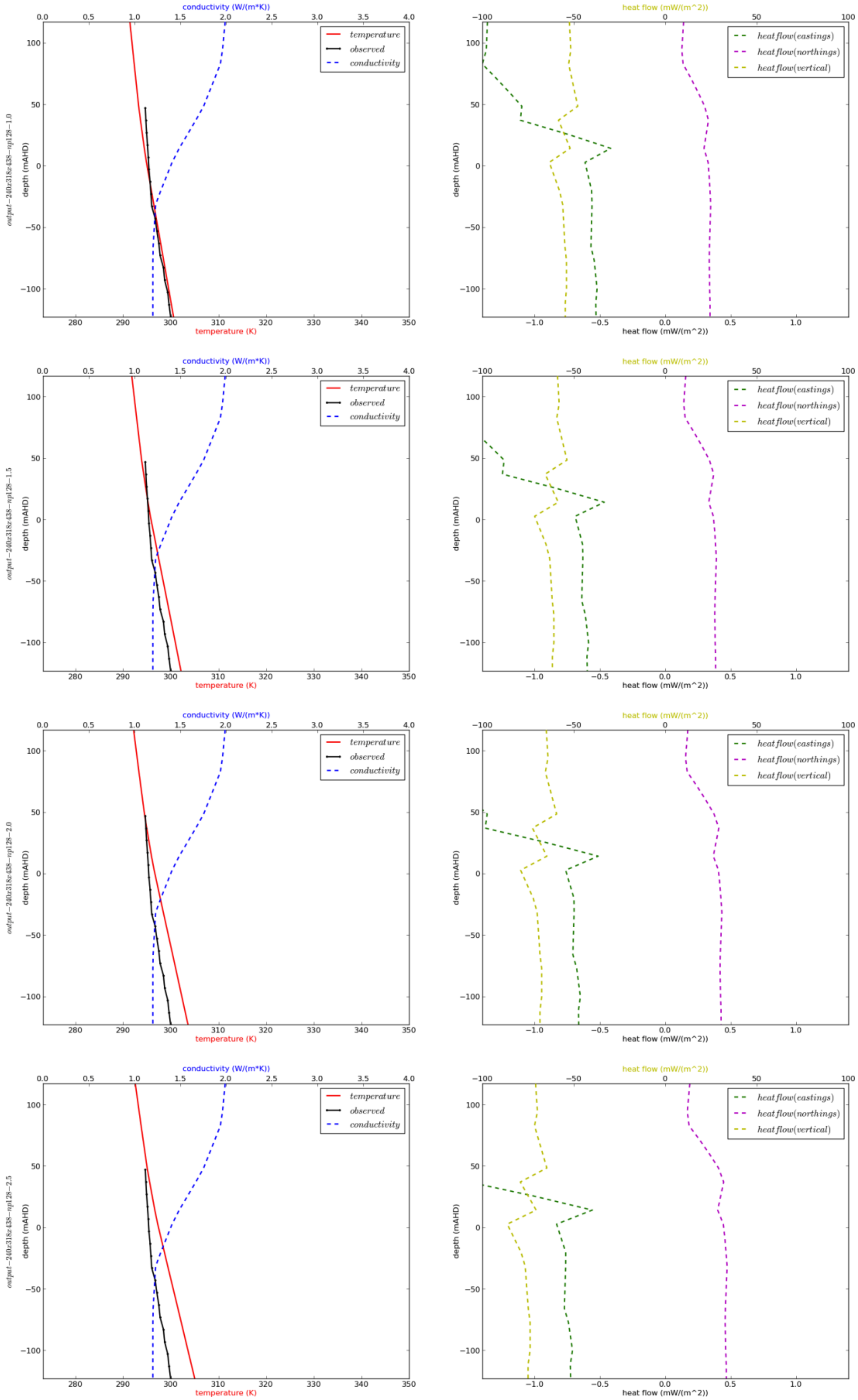
conductivity (W/(m*K))
temperature (K)
depth (mAHD)
temperature
observed
conductivity
heat flow (mW/(m^2))
heat flow(eastings)
heat flow(northings)
heat flow(vertical)
output−240x318x438−np128−1.0
output−240x318x438−np128−1.5
output−240x318x438−np128−2.0
output−240x318x438−np128−2.5

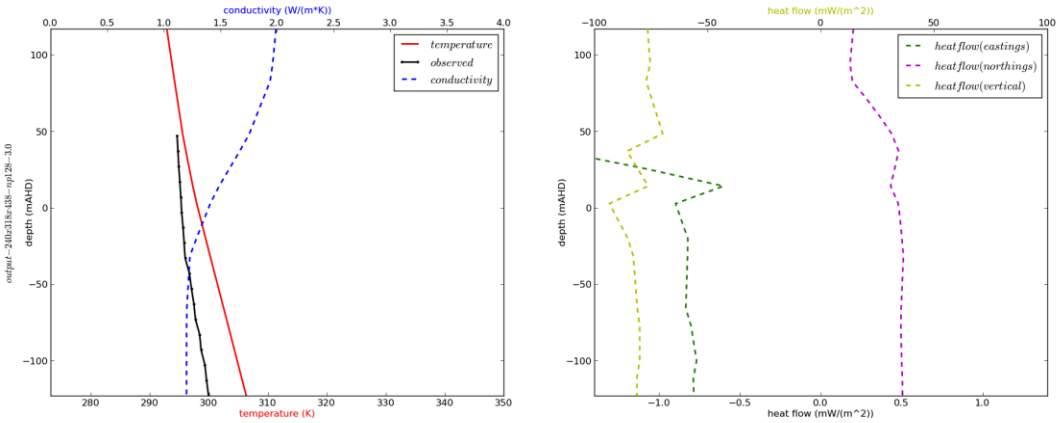

Figure 4 - Profiles for borehole GBD1 (change from sediment to coal/mix unit)

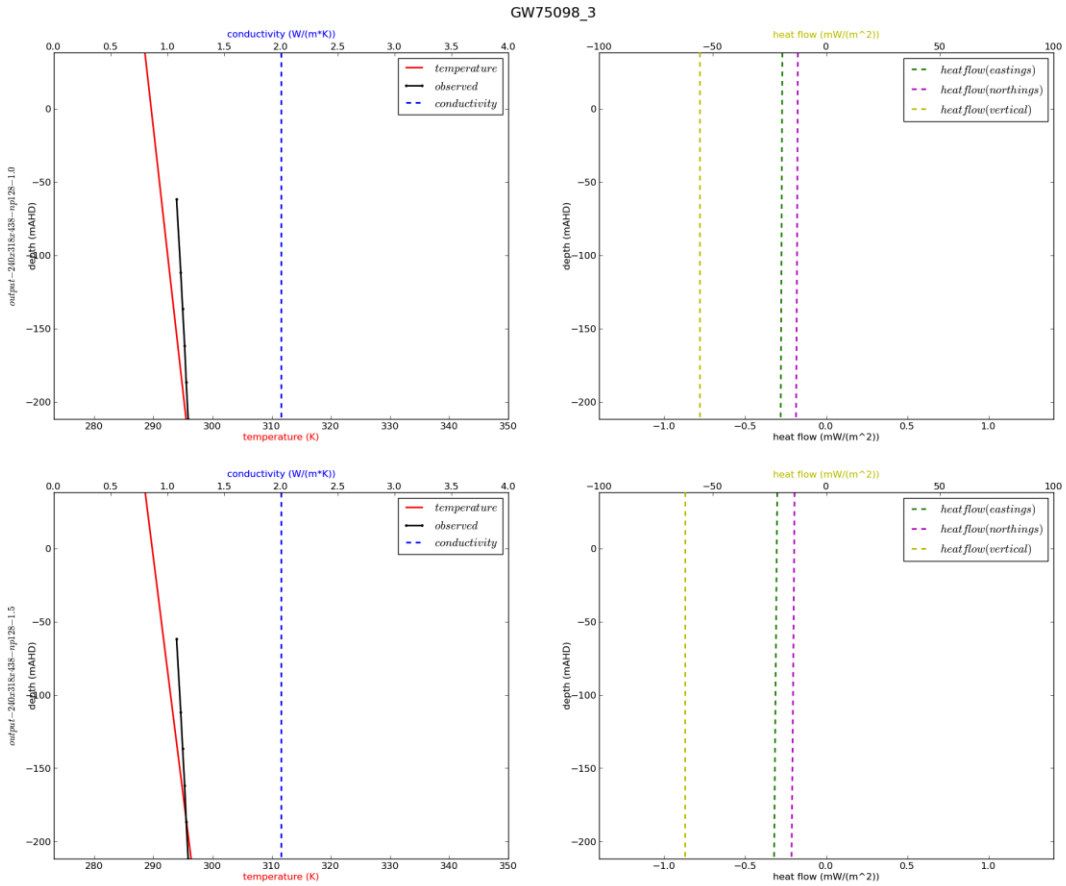

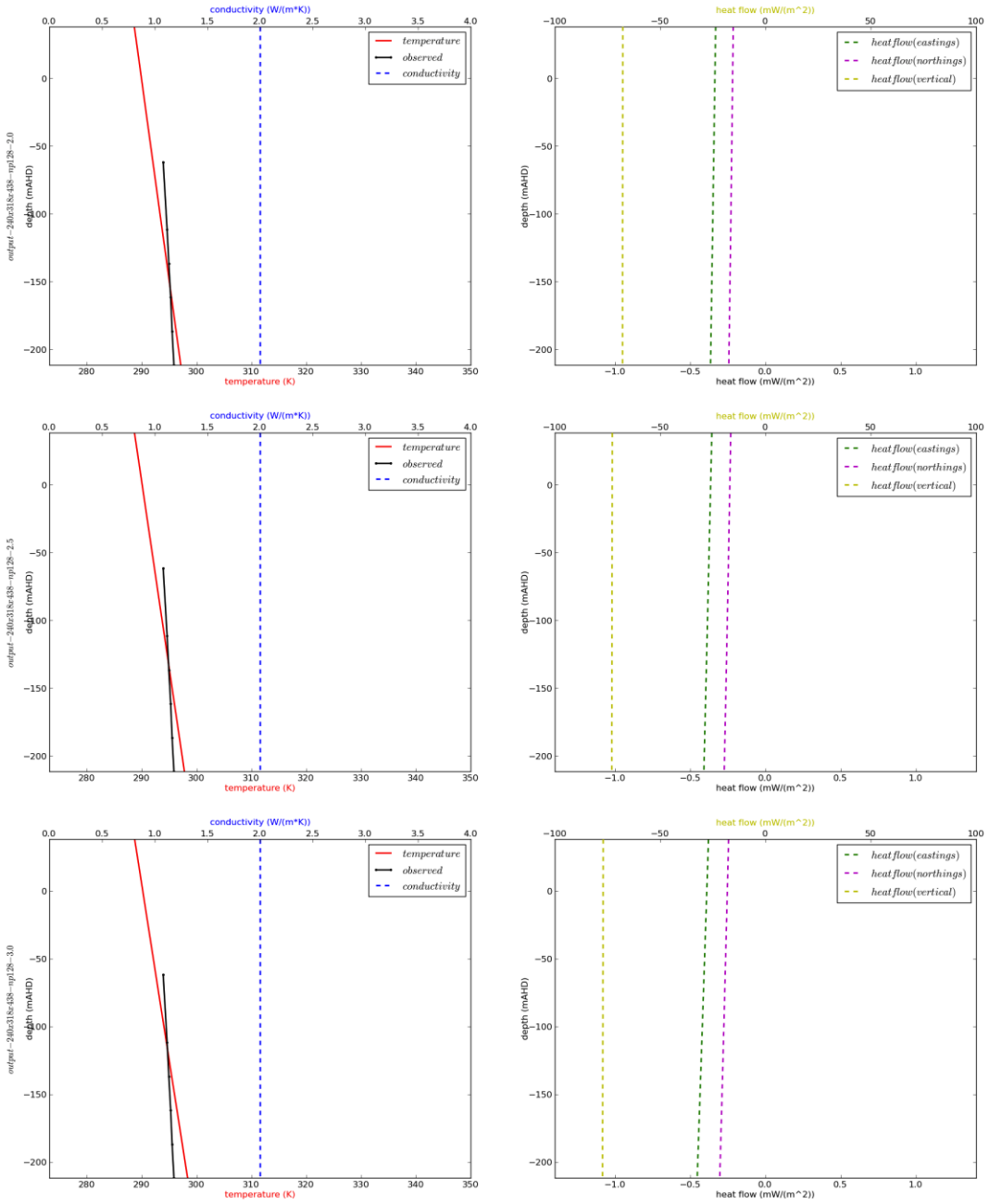

Figure 5 – Profiles for borehole GW75098_3 (no material unit change in borehole)

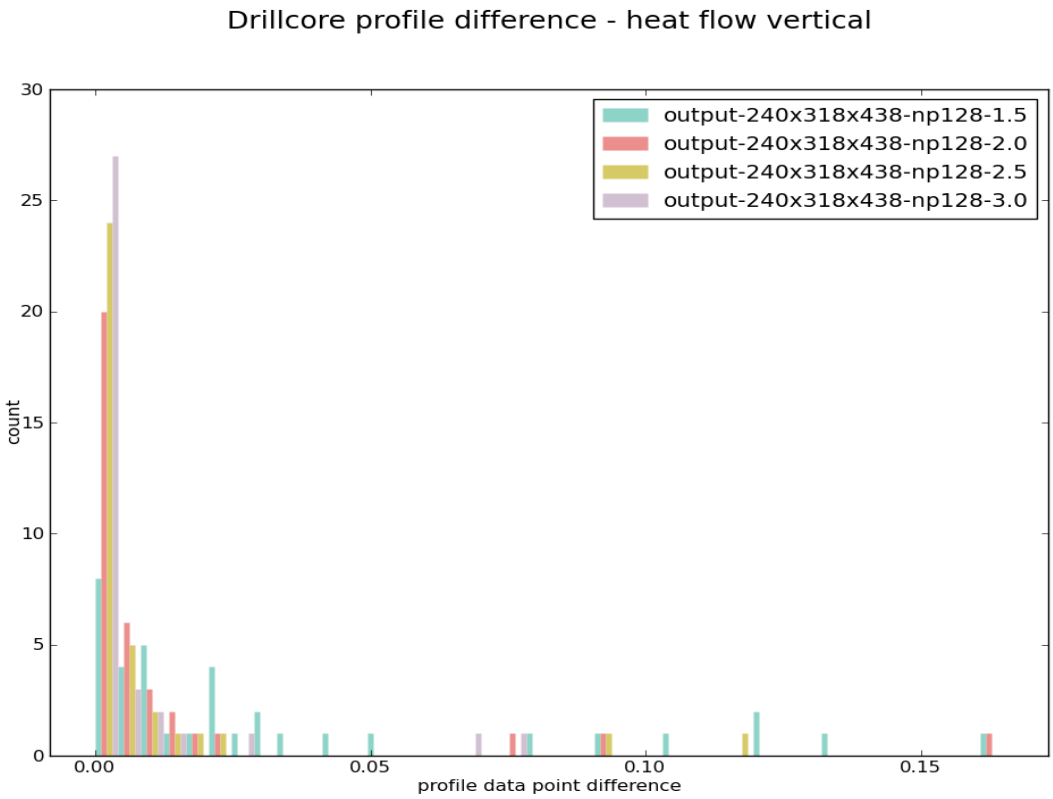

Figure 7 – Regression error of borehole heat flow, vertical component

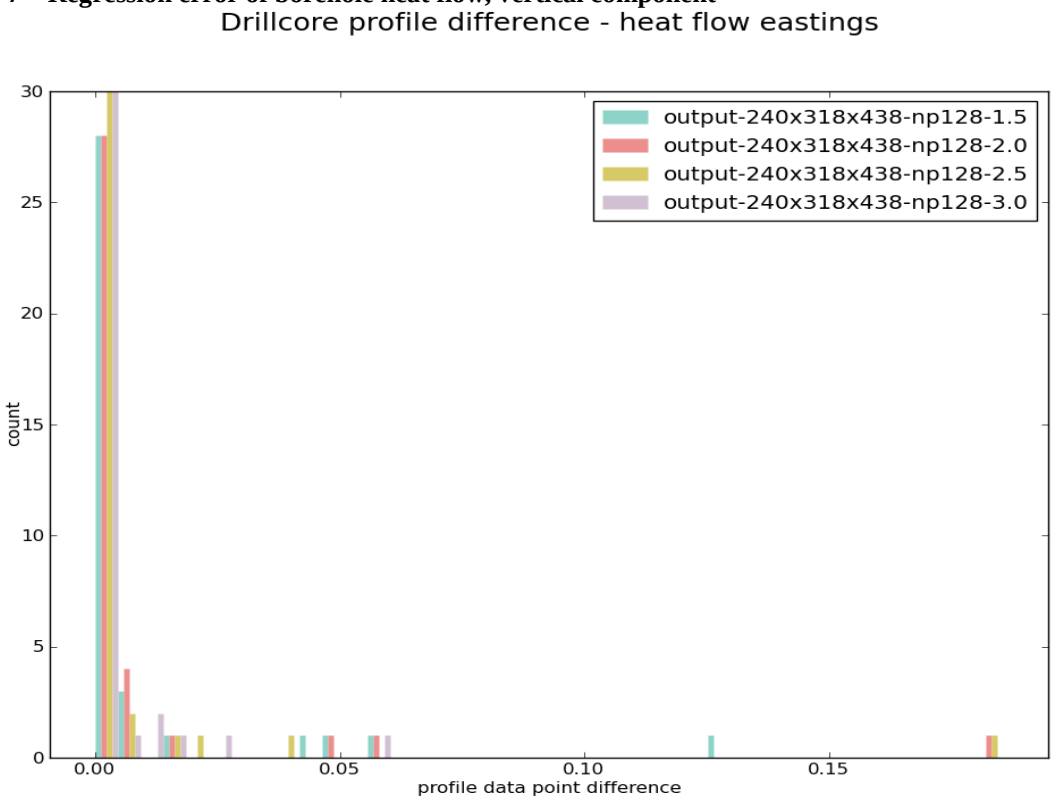

Figure 6 - Regression error of borehole heat flow, eastings component

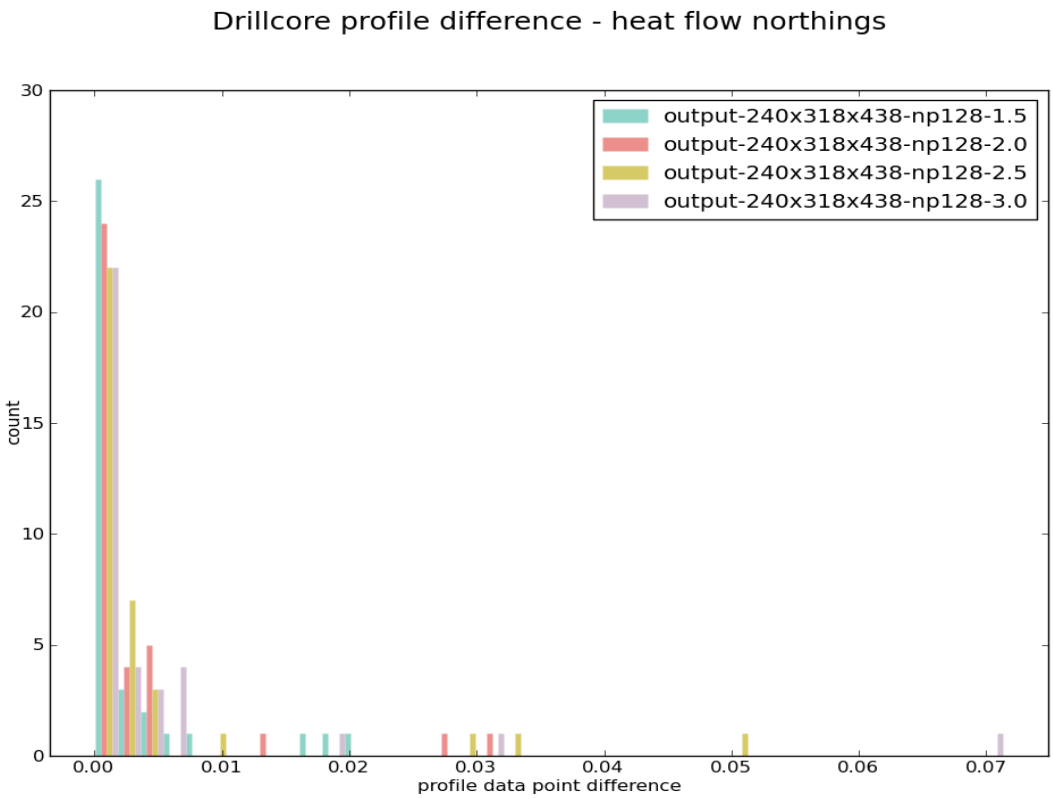

Figure 8 - Regression error of borehole heat flow, northings component